

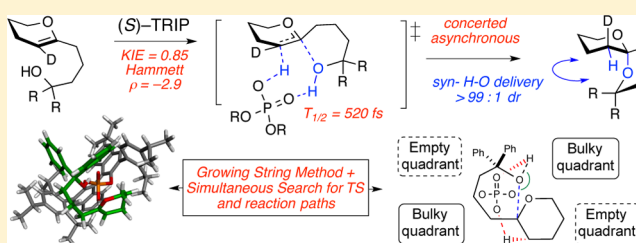
Studies of the Mechanism and Origins of Enantioselectivity for the Chiral Phosphoric Acid-Catalyzed Stereoselective Spiroketalization Reactions

Yaroslav Ya. Khomutnyk, Alonso J. Argüelles, Grace A. Winschel, Zhankui Sun, Paul M. Zimmerman,* and Pavel Nagorny*

Department of Chemistry, University of Michigan, 930 North University Avenue, Ann Arbor, Michigan 48109, United States

S Supporting Information

ABSTRACT: Mechanistic and computational studies were conducted to elucidate the mechanism and the origins of enantiocontrol for asymmetric chiral phosphoric acid-catalyzed spiroketalization reactions. These studies were designed to differentiate between the S_N1 -like, S_N2 -like, and covalent phosphate intermediate-based mechanisms. The chiral phosphoric acid-catalyzed spiroketalization of deuterium-labeled cyclic enol ethers revealed a highly diastereoselective syn-selective protonation/nucleophile addition, thus ruling out long-lived oxocarbenium intermediates. Hammett analysis of the reaction kinetics revealed positive charge accumulation in the transition state ($\rho = -2.9$). A new computational reaction exploration method along with dynamics simulations supported an asynchronous concerted mechanism with a relatively short-lived polar transition state (average lifetime = 519 ± 240 fs), which is consistent with the observed inverse secondary kinetic isotope effect of 0.85. On the basis of these studies, a transition state model explaining the observed stereochemical outcome has been proposed. This model predicts the enantioselective formation of the observed enantiomer of the product with 92% ee, which matches the experimentally observed value.



INTRODUCTION

The transformations leading to the formation of spiroketal (spiroacetal) functionality represent a fundamentally important class of organic reactions, discussion of which can be found in the majority of introductory organic chemistry textbooks.¹ A variety of natural products contain the spiroketal functionality, and the presence of such a moiety is often crucial for their biological activity.^{1–3} Spiroketalization leads to the formation of a new stereogenic center, and its configuration often defines the biological properties of the molecule (Figure 1). Molecules possessing only one stereogenic center arising from the spiroketal moiety are well-documented, and the absolute configuration of such spiroketals may play an important role in determining the biological properties of these natural products. Thus, (*R*)-olean is a fruit fly sex pheromone that is known to act on male fruit flies, whereas its mirror image (*S*)-olean affects female fruit flies.² Even in cases where numerous additional stereocenters are present, the configuration of the spiroketal can be essential for the properties and biological activity of the molecule, as is the case for the cytotoxic natural product pectenotoxin 1, which was found to be more active than its thermodynamically more stable epimer, pectenotoxin 4.³

Numerous studies have investigated factors governing the formation and stability of spiroketals. Typically, the stability of spiroketals is determined by both steric and stereoelectronic effects, and in the absence of significant steric effects,

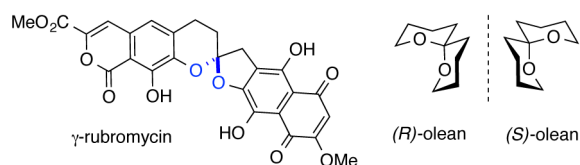
stereoelectronic effects usually play the determining role.⁴ The spiroketalization of dihydroxyketones **1** (Scheme 1) may proceed through either hydroxyacetals **2** or cyclic enol ethers **3** and may lead to diastereomeric spiroketals **4** and **5**. Diastereomer **5** is more thermodynamically stable and is typically the major product under equilibrating conditions. The preference for the formation of thermodynamic product **5** is attributed to a stereoelectronic effect arising from an additional $n(O) \rightarrow \sigma^*(C-O)$ stabilizing interaction that is absent in the nonthermodynamic spiroketal **4**. The majority of natural spiroketals possess thermodynamically favored configurations, which leads to the assumption that their biosyntheses are under thermodynamic control. However, experimental evidence exists to suggest that spiroketal biosyntheses could also happen under enzymatic stereocontrol.⁵

In view of the fact that natural spiroketals prevalently possess the thermodynamically most stable configuration, the majority of synthetic approaches to natural spiroketals rely on catalyst-promoted cyclization under equilibrating conditions.^{6,7} At the same time, similar conditions cannot be employed when a less stable nonthermodynamic configuration is desired (cf. pectenotoxin 1; Figure 1). In those cases, the stereoselective synthesis of spiroketals via direct acetalization becomes significantly more challenging.⁸ Equally challenging is the

Received: December 1, 2015

Published: December 7, 2015

Chiral spiroketals:



Nonthermodynamic spiroketals:

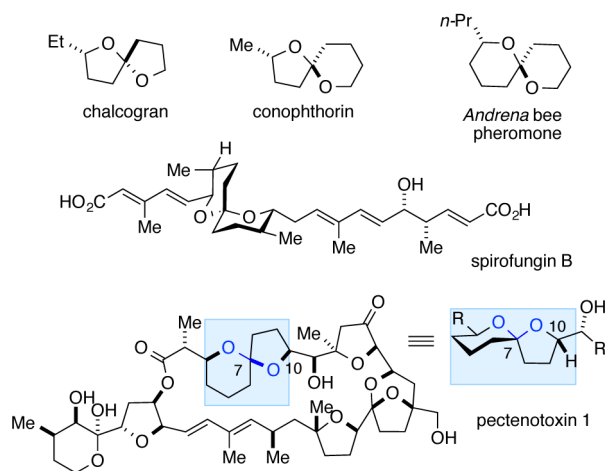
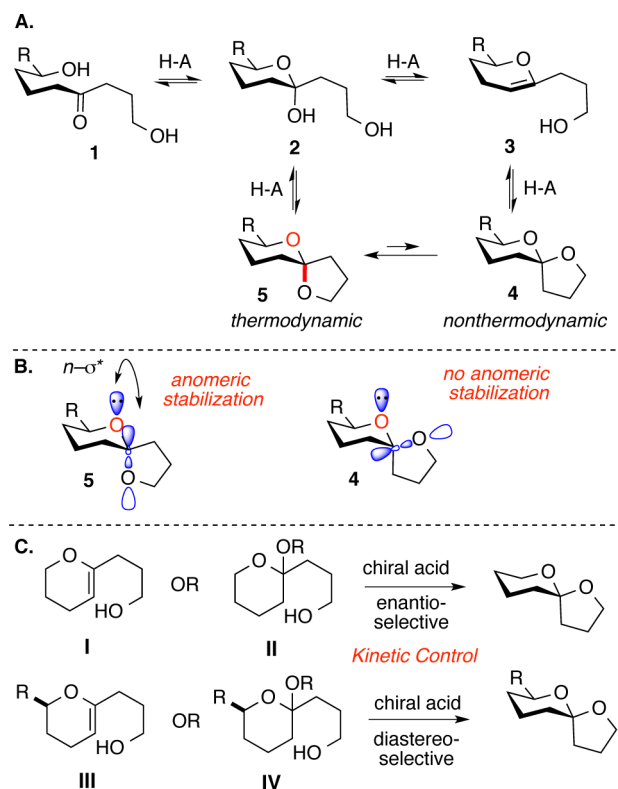


Figure 1. Examples of natural products with spiroketals that are challenging to synthesize.

Scheme 1^a

^a(A) Formation of thermodynamic and nonthermodynamic spiroketals from dihydroxyketones **1** and cyclic enol ethers **3**. (B) Stereoelectronic stabilization of thermodynamic spiroketals. (C) Catalyst-controlled spiroketalizations.

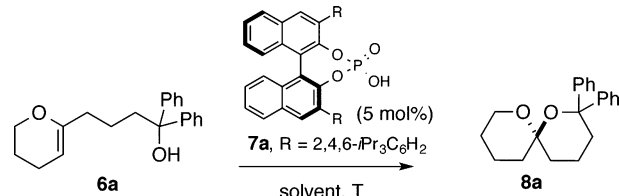
enantioselective synthesis of a spiroketal moiety, in which case the ketal stereocenter is the only source of chirality in the natural product (cf. γ -rubromycin or olean; Figure 1). Most current approaches to nonthermodynamic or chiral spiroketals rely on substrate- or auxiliary-directed methods to form the spiroketal stereocenter.^{8–10} Chiral-reagent-controlled formations of spiroketals are also known but significantly more rare.^{10c} While the direct chiral-catalyst-controlled formation of chiral and nonthermodynamic spiroketals would address the problems specified above, until recently such transformations¹¹ as well as the catalyst-controlled formation of *O,O*-acetals¹² had been unknown. Among the various challenges associated with the use of chiral catalysts, promoting the formation of spiroketals without epimerization of the formed stereocenter and controlling the reactivity of the oxocarbenium ion intermediates could be highlighted as the major challenges to be overcome. Our group has long-standing interests in hydrogen-bond-donor catalysis and its applications to acetalization reactions.^{11b,c,12g,13} Contemporaneously with Coric and List,^{11a} our group^{11b} recently demonstrated that both of these problems can be avoided if chiral phosphoric acids are employed as the catalysts for the cycloisomerization of cyclic enol ethers **I** and **III** under kinetic control. Correspondingly, this article summarizes our work on chiral phosphoric acid (CPA)-catalyzed stereoselective spiroketalizations that could be used to synthesize chiral and nonthermodynamic spiroketal motifs (Figure 1). In addition, this article describes experimental and computational studies directed to elucidation of the mechanism and the origins of enantiocontrol for these reactions. Since many different mechanistic pathways can be proposed for these transformations, the described studies were designed to differentiate among these pathways and to gain information about the reactive intermediates. Thus, the cyclization of deuterated cyclic enol ethers, Hammett studies, and secondary kinetic isotope effect (KIE) studies were employed to differentiate between the S_N1 -like, S_N2 -like, and covalent phosphate intermediate-based mechanisms. These studies suggest that the CPA-catalyzed cyclizations happen via a polar concerted mechanism that does not involve long-lived oxocarbenium intermediates. A new computational reaction exploration method along with molecular dynamics computational studies independently validated this proposal and served to derive a transition state model explaining the observed stereochemical outcome.

RESULTS AND DISCUSSION

Initial Optimization Studies. Although CPAs had been previously employed to catalyze the formation of chiral *N,N*-,^{14a–c,e} *N,O*-,^{14d} *N,S*-,^{14e,f} and simple *O,O*-acetals,¹² no examples of a successful chiral-catalyst-controlled enantioselective or diastereoselective spiroketalization existed at the beginning of these studies. Despite these encouraging precedents, the prospects of using chiral Brønsted acids to promote catalyst-controlled spiroketalizations were unclear considering that spiroketals are significantly more prone to epimerization under acidic conditions. With this in mind, we surmised that the use of cyclic enol ether **I** or **III** as the spirocyclization precursor was key in developing this transformation, as the mixed acetal precursors **II** and **IV** (Scheme 1) are too similar to spiroketals in their ability to ionize under the acidic conditions. Cycloisomerization of enol ethers **I** and **III** is easier to achieve under epimerization-free conditions, and the Deslongchamps and Pihko groups had previously utilized weak

acids such as acetic acid ($pK_a = 4.7$, H_2O) to promote kinetic spiroketalizations.¹⁵ The same studies also indicated that the reactions catalyzed by stronger trifluoroacetic acid ($pK_a = -0.25$, H_2O) proceeded under thermodynamic control. At the same time, we surmised that the chiral phosphoric acids have intermediate acidities ($pK_a \sim 2$, H_2O) and would be excellent catalysts for kinetic spiroketalizations. In order to evaluate the feasibility of this proposal, spiroketalization of substrate **6a** to give **8a** was investigated (Table 1).^{11b} Commercially available

Table 1. Initial Evaluation of the Enantioselective Spiroketalization Reaction Conditions^a



entry	solvent	T	time, h ^b	conversion (yield), %	ee, %
1	CH ₃ CN	rt	0.5	100 (93)	7
2	THF	rt	12 ^c	30 (25)	10
3	EtOAc	rt	12	100 (98)	16
4	benzene	rt	1	100 (99)	24
5	toluene	rt	1	100 (98)	25
6	CCl ₄	rt	1	100 (96)	40
7	hexanes	rt	0.5	100 (98)	63
8	cyclohexane	rt	0.5	100 (95)	60
9	pentane	rt	0.5	100 (97)	69
10	pentane	0 °C	4	100 (97)	73
11	pentane	-35 °C	40	100 (96)	66
12	pentane, 4 Å MS	0 °C	14	100 (97)	84
13	pentane, 4 Å MS	-35 °C	40	100 (96)	92

^aPhosphoric acids were washed with 6 M HCl after purification by column chromatography. Unless specified otherwise, reactions were performed on a 0.1 mmol scale (0.02 M solution). ^bTime required for the reaction to reach completion. ^cIncomplete conversion.

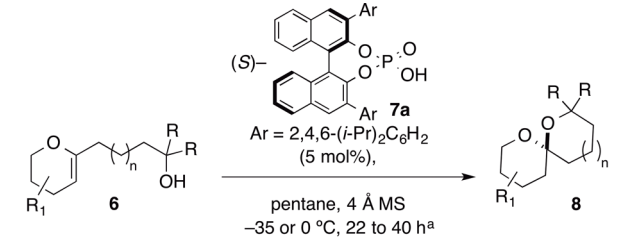
(S)-TRIP (**7a**) was selected as the initial catalyst for the reaction optimization (Table 1); however, our subsequent attempts to identify a superior catalyst for this reaction were not successful (cf. Table S1 in the Supporting Information).

In our attempts to optimize the selectivity for the formation of **8a**, we encountered significant solvent effects (Table 1). The reactions conducted in higher-polarity solvents (entries 1–5) resulted in lower levels of stereocontrol, while oxygenated solvents such as tetrahydrofuran (THF) and ethyl acetate significantly retarded the rate of cyclization (entries 2 and 3). At the same time, the spiroketalizations conducted in nonpolar hydrocarbon solvents (entries 7–9) proceeded with higher enantioselectivities and shorter reaction times. The observed solvent effects emphasize the significance of non-covalent interactions between the substrate and chiral phosphoric acid for the productive reaction pathway. More polar, oxygenated solvents (entries 2 and 3) can competitively form hydrogen bonds with the CPA, thereby reducing the complexation with **6a**. At the same time, the less polar solvents favor enhanced hydrogen bonding and other types of non-covalent interactions between **6a** and **7a**. On the basis of these arguments, we surmised that the selectivity for the formation of **8a** could be further enhanced at lower reaction temperatures and if the

hydrogen-bonding impurities such as water were removed. Although lowering the reaction temperature alone did not significantly affect the enantioselectivity (entries 10 and 11), the addition of 4 Å MS combined with lowering the temperature to -35 °C resulted in the formation of **8a** with 92% ee (entry 13).

Enantioselective and Diastereoselective Spiroketalizations. After the optimal reaction conditions were identified, the scope of the enantioselective spiroketalization was evaluated next (Table 2). In addition to the previously evaluated **6a**, the

Table 2. Investigation of the Substrate Scope of Enantioselective Spiroketalization^a



8a	8b^b	8c	
96%, 92% ee	81%, 93% ee	96%, 94% ee	
8d^b	8e^b	8f^b	8g^b
93%, 96% ee	89%, 90% ee	82%, 75% ee	88%, 74% ee
8h	8i	8j	8k
87%, 62% ee	92%, 4% ee	89%, 5% ee	72%, 54% ee

Ar = 4-(MeS)Ph

X-Ray

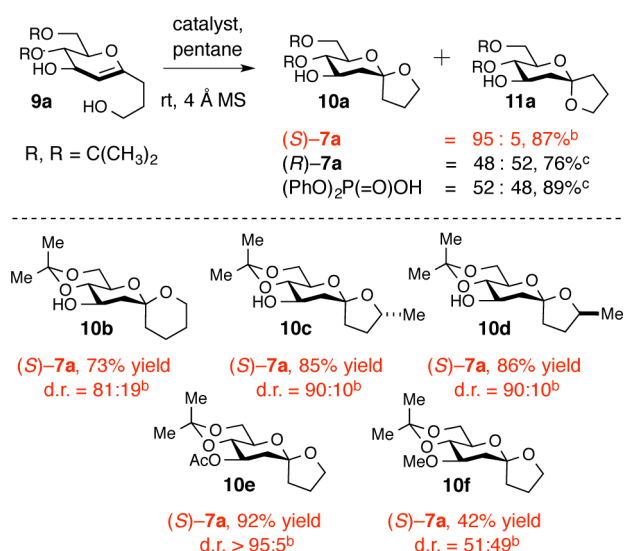
^aReactions were performed on a 0.1–0.05 mmol scale (0.02 M solution), and the selectivities of these reactions were found to be scale-independent. Catalyst (S)-**7a** was used, unless otherwise noted. ^bThe reaction was conducted with catalyst (R)-**7a**.

cyclic enol ethers **6b–k** were synthesized and subjected to the cyclizations leading to **8b–k**. The introduction of *p*-MeS substituents on the aromatic rings in **6b** and the extension of the tether length in **6c** did not affect the reaction yield and selectivity for the corresponding products **8b** and **8c**. Similarly, the introduction of a fused benzene ring into the side chain (**6d**) or into the enol ether ring (**6e**) was well-tolerated, and the corresponding products were obtained in excellent selectivities and yields. At the same time, the cyclization of analogous substrates **6f–h** containing less rigid Bn substituents at the tertiary alcohol consistently exhibited lower enantioselectivities. Cyclization leading to **8g** was found to be more selective (88% yield, 74% ee) than a similar reaction leading to **8h** that lacks a methyl group on the aromatic ring (87% yield, 62% ee). These

results indicate that further variations in the substrate backbone can potentially enhance the selectivity of the substrates lacking Ph substitution at the nucleophile. This is further reinforced by the observation that primary-alcohol-containing precursor **6k** could be cyclized enantioselectively to give **8k** (72%, 54% ee) while the reactions with similar substrates **6i** and **6j** led to almost unselective formation of the corresponding spiroketals **8i** and **8j**.

The results summarized in Table 2 indicate that a chiral catalyst can control the selectivity of the cyclization of achiral substrates **6**. However, because the chirality of the substrate may completely override the course of cyclization dictated by the catalyst, the effect of the catalyst on the cyclization of chiral substrates had to be addressed next (Scheme 2).^{11b} Since the

Scheme 2. CPA-Controlled Formation of Nonthermodynamic Spiroketals^a



^aThe reactions with (S)-**2a** (5 mol %) and (R)-**2a** (5 mol %) were performed for 14 h, and the reactions with (PhO)₂PO₂H (10 mol %) were performed for 2 h. Longer exposure to (PhO)₂PO₂H (10 mol %) resulted in complete equilibration to give the thermodynamic spiroketals. The cyclizations of **9a** were performed on different scales without significant variation in selectivity. ^bYield of nonthermodynamic spiroketal **10**. ^cCombined yield of **10** and **11**.

reactions of carbohydrate-based oxocarbenium ions are highly sensitive to stereoelectronic and steric effects, conformationally locked D-glucal derivatives (e.g., **9a**) were selected for these studies. Upon spiroketalization, these substrates can provide anomericly stabilized thermodynamic products such as **11a** or less stable nonthermodynamic spiroketals (**10a–f**). Thus, to evaluate the effect of the chiral catalyst on the course of these cyclizations, substrate **9a** was subjected to treatment with (S)-**7a**, (R)-**7a**, or the achiral catalyst (PhO)₂PO₂H. Remarkably, the treatment of glycal **9a** with catalyst (S)-**7a** (5 mol %) resulted in a highly diastereoselective cyclization, leading to nonthermodynamic spiroketal **10a** (95:5 dr). At the same time, the exposure of **9a** to (R)-**7a** or (PhO)₂PO₂H provided ~1:1 mixtures of nonanomeric and anomeric products **10a** and **11a**, clearly indicating that the chirality of the catalyst is essential for the selective formation of **10a**. Similar trends were observed for other substrates, and catalyst (S)-**7a** was used for the highly diastereoselective formation of various nonthermodynamic spiroketals (**10a–e**) in good yields and diastereoselectivities.

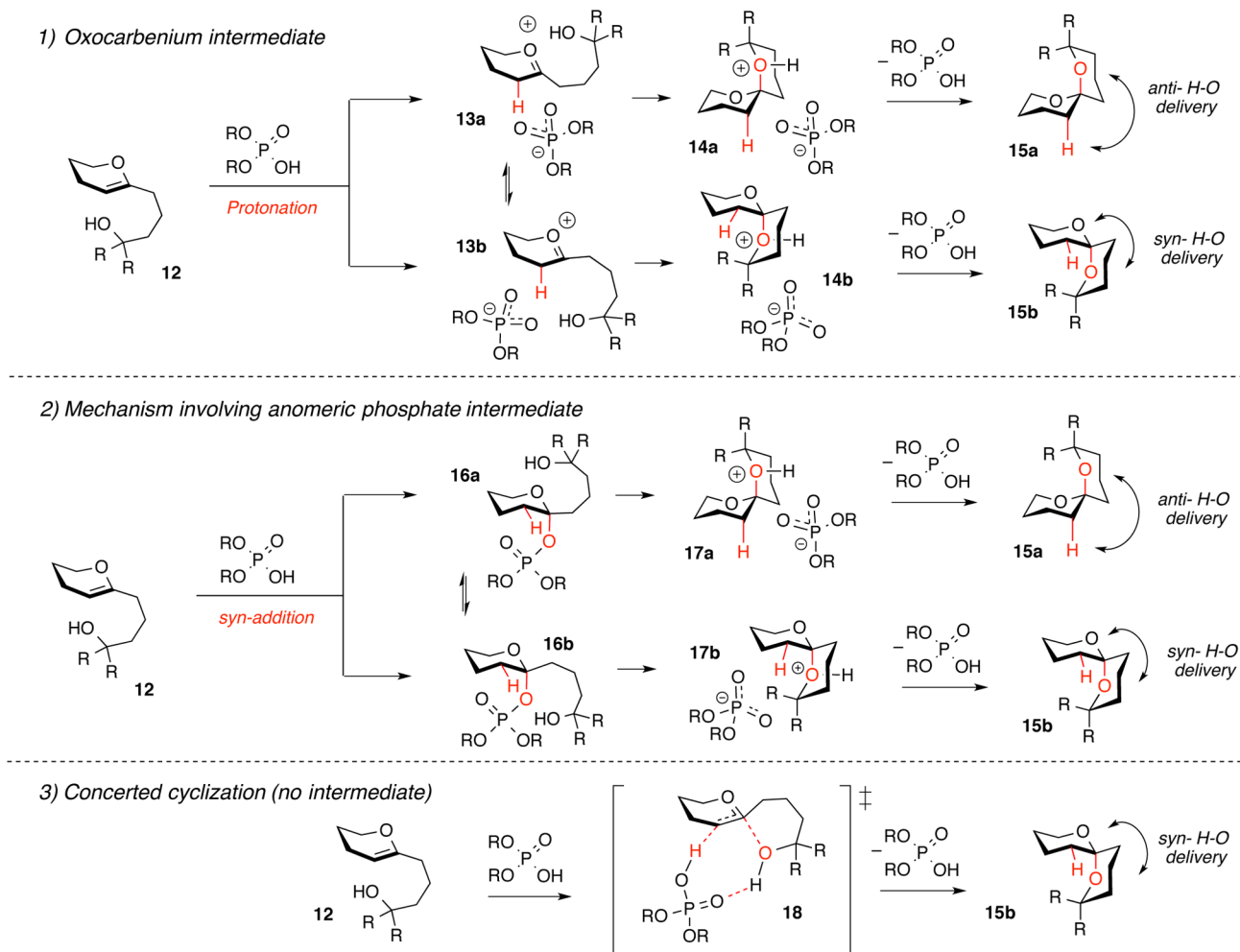
Interestingly, the nature of the protecting group at C3 was found to play an important role, and, unlike the formation of **10e**, the cyclization leading to **10f** was not selective.

The results summarized in Scheme 2 suggest that the cyclizations catalyzed by **7a** proceed under kinetic conditions. The non-anomeric spiroketals **10** are clearly stable toward both enantiomers of acids **7a** for the duration of the reaction (i.e., 14 h). At the same time, when pure **10a** was treated with (S)-**7a** under the reaction conditions, complete epimerization to give **11a** was observed after 60 h.

Mechanistic Considerations. The above results suggest that **7a** is the catalyst of choice for the asymmetric spiroketalization of tertiary-alcohol-containing substrates **6** as well as for the diastereoselective cyclization of chiral substrates **9** leading to non-anomeric spiroketals **10**. Interestingly, the larger size of glycals **9** excluded the requirement of using the tertiary-alcohol-based nucleophiles, and **7a** could promote the cyclizations leading to **10** with primary and secondary alcohols as nucleophiles with good-to-excellent selectivities. However, although the aforementioned results provide some crude idea about the scope and limitation of the method, the mechanistic and stereochemical models explaining the origins of the stereocontrol are essential for more general use of these and related transformations.

Despite the fact that CPA-catalyzed transformations invoking oxocarbenium ion intermediates have received significant attention in recent years, very few attempts to understand the mechanisms of such transformations and the factors governing the selectivity have been made.¹⁶ The formation of stable oxocarbenium ion intermediates has been proposed in the recent computational studies of *N*-triflyl phosphoramidate-catalyzed cyanohydrin ether formation^{16a} and CPA-catalyzed Petasis–Ferrier rearrangements.^{16b} However, instances where theoretical studies identified alternative mechanisms not involving the formation of oxocarbenium ion intermediates have also been documented. Thus, the recent studies of the acid-catalyzed enantioselective formation of pyrrolidines by the Toste group¹⁷ and piperidines by our groups^{13d} identified alternative pathways involving covalently linked thiophosphate (or phosphate) intermediates rather than the corresponding high-energy carbenium or oxocarbenium ion pairs. The oxocarbenium-based mechanisms for acid-catalyzed acetal formation have indeed received widespread acceptance; however, transformations of this type not involving oxocarbenium ion intermediates have also been documented. Accordingly, the Tan group observed an S_N2-like concerted (rather than S_N1-like oxocarbenium-based) mechanism for the methanol-promoted spirocyclization of glycal epoxides.¹⁸ In line with these findings is the theoretical study of the thiourea-catalyzed tetrahydropyranation reaction by Kotke and Schreiner,¹⁹ in which a concerted asynchronous addition of alcohol nucleophiles rather than the formation of a discrete oxocarbenium ion intermediate is proposed. Similarly, the true nature of the glycosylation reaction intermediates has been a subject of long-standing debates.²⁰ Both the ionic S_N1-like and concerted S_N2-like mechanisms are commonly invoked to explain the outcome of glycosylation reactions, and there is strong evidence that nonionic mechanisms are operational in some instances. For example, the Crich group has provided overwhelming evidence demonstrating that 4,6-*O*-benzylidene-directed β-mannosylation reactions proceed through covalently bound glycosyl triflates rather than through discrete glycosyl oxocarbenium ion intermediates.²¹

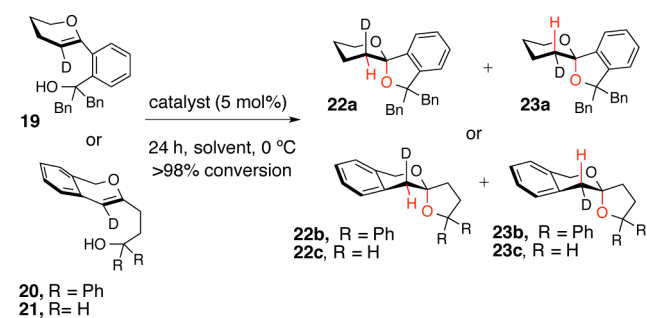
Scheme 3. Potential Mechanisms of CPA-Catalyzed Spiroketalizations



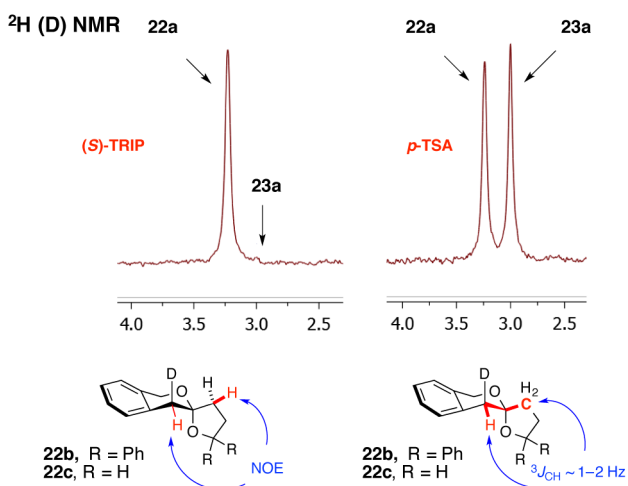
With these prior observations in mind, we considered several different mechanistic pathways for the CPA-catalyzed enantioselective spiroketalization reaction (Scheme 3). The reaction mechanisms proceeding through an oxocarbenium ion or covalently linked phosphate intermediate and a concerted mechanism with concomitant C–H and C–O bond formation were viewed as the most prominent options. Both the counterion orientation and the relative stereochemistry of the forming C–H and C–O bonds are crucial for understanding the origins of stereoinduction and developing a stereochemical model. At the same time, these important factors are typically omitted from the mechanistic considerations. Thus, to our knowledge, no information on the selectivity of the C–H/C–O bond addition has been available prior to this work. In theory, the cyclization proceeding via an oxocarbenium ion intermediate can occur through two different modes. In the first mode of cyclization, the C–H and C–O bonds form from different faces of the molecule (i.e., the pathway proceeding through 13a/14a/15a). Alternatively, the pathway proceeding through 13b/14b/15b and resulting in syn protonation/C–O bond formation can be envisioned. Similarly, the reaction proceeding through the anomeric phosphate intermediate conformation 16a or 16b can happen through a retentive or inversive (S_N2 -like) mechanism. An anti relationship between the formed C–H and C–O bonds is expected for the inversive mechanism (i.e., the 16a/17a/15a pathway), and a syn

relationship between the formed C–H and C–O bonds is expected for the retentive mechanism (i.e., the 16b/17b/15b pathway). Unlike in the aforementioned mechanistic options that may lead to both selective product formation and mixtures of syn and anti products, the concerted mechanism, in which the phosphoric acid acts as the bifunctional catalyst, can produce only the syn product 15b (Scheme 3).

Studies of Diastereoselective Cyclizations. With these considerations in mind, we designed and conducted experiments to distinguish between the diastereodivergent syn and anti spiroketalization modes (Scheme 4). To obtain this information, we generated deuterated cyclic enol ethers 19–21 and subjected them to the cyclization in a nonpolar solvent (i.e., toluene, dichloromethane, or pentane) using (*S*)-7a, chloroacetic acid, $\text{CF}_3\text{CO}_2\text{H}$, or *p*-toluenesulfonic acid (*p*-TSA) as the catalyst. The outcomes of these reactions were monitored using ^2H (D) NMR (107 MHz). As per our discussion above (i.e., Scheme 3), the cyclization of 19 may lead to the syn product 22a or the anti product 23a. Similarly, the cyclizations of 20 and 21 may provide the syn diastereomers 22b and 22c or the anti diastereomers 23b and 23c, respectively. Remarkably, only the syn products 22a–c were detected in the experiments with weaker acids (i.e., (*S*)-7a and $\text{ClCH}_2\text{CO}_2\text{H}$; Scheme 4, entries 1–5); however, unselective formation of the syn and anti products was detected for the *p*-TSA and $\text{CF}_3\text{CO}_2\text{H}$ -catalyzed reactions (entries 6 and

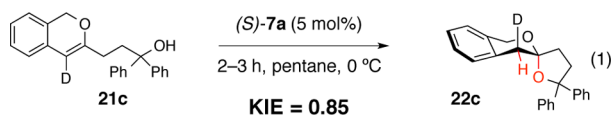
Scheme 4. Diastereoselective Spiroketalization of Deuterium-Labeled Substrates^a

entry	catalyst	solvent	22a : 23a	22b : 23b	22c : 23c
1	(S)-7a	toluene	99 : 1	99 : 1	99 : 1
2	(S)-7a	CH ₂ Cl ₂	99 : 1	99 : 1	99 : 1
3	(S)-7a	pentane	99 : 1	99 : 1	99 : 1
4	ClCH ₂ CO ₂ H ^b	pentane	99 : 1	99 : 1	99 : 1
5	ClCH ₂ CO ₂ H ^b	CH ₂ Cl ₂	99 : 1	99 : 1	— ^c
6	<i>p</i> -TSA ^d	CH ₂ Cl ₂	1 : 1	1 : 1	1 : 1
7	CF ₃ CO ₂ H ^d	pentane	1 : 1	1 : 1	1 : 1



^aThe reactions were performed on a 0.5–0.05 mmol scale, and each experiment was reproduced twice. D (²H) NMR spectra were recorded at 107 MHz using a Varian VNMRs-700 spectrometer. The observed diastereoselectivities were found to be conversion-independent. ^b10 mol % catalyst was employed. ^cNo reaction was observed. ^dThe racemization reactions were found to be faster than the cyclization reactions under these conditions.

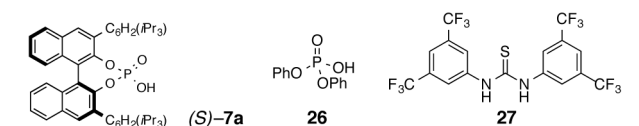
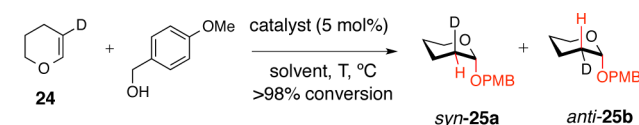
7). The absence of the selectivity for the *p*-TSA-catalyzed reactions is attributed to rapid epimerization under the cyclization conditions. Thus, subjecting diastereomerically pure **22b** to *p*-TSA at –40 °C resulted in rapid isomerization to a 1:1 mixture of **22b** and **23b** after 15 min. Finally, a substantial inverse kinetic isotope effect (KIE = 0.85) was observed for the cyclization of **21c** into **22c** (cf. eq 1).



The relative configurations of **22a–c** were established using nuclear Overhauser effect (NOE) and two-dimensional heteronuclear NMR studies, including ³J_{CH} determination by

SeLEXSIDE,²² and some of the key signals are depicted in Scheme 4 (see the Supporting Information for additional details). Despite the numerous studies on the spiroketalization mechanism and the widespread use of spiroketals in organic synthesis, the results in Scheme 4 represent the first documented evidence suggesting that the kinetic spiroketalization of cyclic enol ethers in nonpolar solvents proceeds via highly selective syn H–O addition.

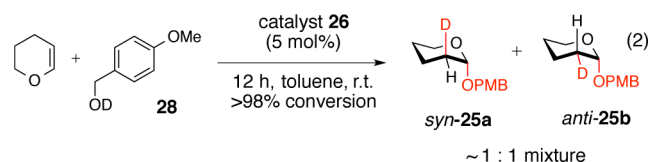
To investigate whether the syn addition is more general and could be observed in intermolecular acetalization reactions, the reaction of D-labeled dihydropyran (**24**) and *p*-methoxybenzyl alcohol was investigated next (Table 3). As in the

Table 3. Acetalization with 3,4-Dihydro-2H-pyran-5-d^a

entry	catalyst	solvent	T	time, h	syn-25a:anti-25b
1	(S)-7a	CH ₂ Cl ₂	rt	12	1:1
2	26	pentane	0 °C	48	1:1
3	26	benzene	rt	12	1:1
4 ^b	ClCH ₂ CO ₂ H	neat	rt	48	—
5 ^c	27	benzene	0 °C	42	1:1

^aThe reactions were performed on a 0.15–0.59 mmol scale, and each experiment was reproduced twice. D (²H) NMR spectra were recorded at 107 MHz on a Varian 700 spectrometer. The observed diastereoselectivities were found to be conversion-independent. ^bNo reaction was observed with 10 mol % catalyst. ^c2 mol % catalyst **27** was employed.

spiroketalization studies with deuterium-labeled cyclic enol ethers, the formation of two diastereomeric products, *syn*-**25a** and *anti*-**25b**, is also expected in this case. The phosphoric acids (S)-**7a** and **26**, chloroacetic acid, and Schreiner's thiourea **27** were selected as the catalysts. The formation of **25** promoted by these catalysts is expected to be irreversible (i.e., kinetic) under most conditions since the tetrahydropyran (THP)-acetals possess significantly higher stability than typical spiroketals. Interestingly, tetrahydropyranlation reactions were found to be dissimilar to spiroketalization reactions. Thus, the reaction of *p*-methoxybenzyl alcohol with **24** produced an approximately 1:1 mixture of products with Brønsted acids (S)-**7a** and **26** (entries 1–3), but no reaction was observed with chloroacetic acid (entry 4). Similar results were observed when unlabeled dihydropyran was reacted with deuterium-enriched *p*-methoxybenzyl alcohol (**28**) using diphenylphosphoric acid **26** as the catalyst (eq 2).



As before, the nonselective formation of both *syn* and *anti* products was observed in this case. Tetrahydropyranylation of methanol catalyzed by thiourea catalyst **27** has been investigated computationally, and the concerted asynchronous addition of methanol proceeding through a polar transition state with oxyanion hole stabilization by **27** has been proposed (*vide supra*).¹⁹ Considering that a concerted asynchronous addition of an alcohol to dihydropyran **24** should result in the selective formation of *syn*-**25a**, we decided to investigate the outcome of the thiourea **27**-catalyzed formation of **25** (Table 3, entry 5). Surprisingly, **27**-catalyzed acetalization of **24** and *p*-methoxybenzyl alcohol produced an equimolar mixture of *syn*-**25a** and *anti*-**25b** in benzene. Since the formation of *syn*-**25a** and *anti*-**25b** is not reversible under the reaction conditions, the outcome of the experiments in Table 3 is consistent with the formation of a relatively long-lived, solvent-separated (rather than contact), oxocarbenium/stabilized alkoxide ion pair. This ion pair could undergo nonselective association, and both faces of oxocarbenium ion are equally exposed to the reaction with the oxyanion nucleophile.

Hammett Studies. The above results indicate that the intramolecular and intermolecular acetalization reactions proceed through different mechanisms. To further differentiate between the mechanistic options outlined in Scheme 3, a Hammett study was executed for the cyclization of aromatic enol ethers **29** leading to spiroketals **30** (Figure 2). Thus, the rate constants for the cyclizations of substrates **29** with either electron-withdrawing (i.e., X = Cl, F) or electron-donating (i.e.,

X = CH₃O, CH₃) substituents as well as the unsubstituted substrate (X = H) were measured at low conversion (Figure 2A). The obtained $\log(k_{\text{obs}}/k_{\text{H}})$ values for the electronically varied substrates **29** displayed an excellent linear correlation ($R^2 = 0.98$) when plotted against the corresponding known σ values. These results allowed for the measurement of ρ value to be -2.9 , which is consistent with a buildup of positive charge in the transition state (TS) of the rate-limiting step ($\rho < -1$). It should be noted that the obtained ρ value is lower than the one expected for an S_N1-like mechanism involving rate-limiting formation of a fully charged oxocarbenium ion intermediate. In this regard, the Tan group has investigated the acid-catalyzed epimerization of kinetic D-glucal-derived spiroketals structurally similar to **29** and obtained $\rho = -5.1$, which is more in line with a rate-limiting ionization step than the ρ value obtained in these studies.

The results of the aforementioned studies shed some light on the mechanism of the CPA-catalyzed spiroketalization reactions. Thus, the observed highly diastereoselective *syn* H–O delivery, the significant inverse secondary KIE of 0.85 for substrate **21c** (eq 1) indicating that rehybridization happens in the rate-limiting step, and the accumulation of positive charge in the TS of the rate-limiting step observed in the Hammett study all speak against the formation of the covalent anomeric phosphate intermediates **16** (Scheme 3). This is further reinforced by the fact that *syn* H–O delivery is observed not only for the phosphoric acid catalysts but also for chloroacetic acid. The relatively small ρ value and diastereoselective *syn* H–O delivery are also not consistent with the long-lived oxocarbenium ion intermediates **13** but are more in accord with a highly asynchronous concerted mechanism proceeding through the polarized TS **18** (Scheme 3). At the same time, the scenarios involving the formation of short-lived oxocarbenium/phosphate contact ion pair **13b** or phosphate **16** cannot be completely ruled out with the obtained experimental data. These distinctions, however, can be done on the basis of density functional theory calculations and molecular dynamics studies that would help to identify the pathway with the lowest energy and provide information on the average lifetime of the TS or intermediate involved. With these considerations in mind, we undertook the studies described in the next section.

Computational Studies. Asymmetric spiroketalization with chiral phosphoric acids may proceed through one or more of the mechanisms depicted in Scheme 3, of which the most classical one is mediated by an oxocarbenium intermediate. Experimental analysis of the mechanism provided strong evidence against *anti* H–O delivery (to yield **15a**), but the mechanisms resulting in **15b** could not be ruled out. To gain further insight into the mechanism, the transformation was studied in depth using quantum-chemical calculations.

Reaction mechanisms in relatively large systems with many flexible degrees of freedom—such as the present catalytic system—are especially difficult to characterize using reaction path optimization tools. To overcome these challenging cases, the Zimmerman group developed the growing string method (GSM) to simultaneously search for reaction paths and transition states.^{23a,c,d} By restricting the search to find a transition state within a series of structures along a minimum-energy path from reactants to products, GSM can efficiently locate transition states on highly flat energy surfaces. When our tools were applied to the asymmetric CPA-catalyzed formation of piperidines, an accurate description of the reaction selectivity was obtained that invoked a two-step mechanism proceeding

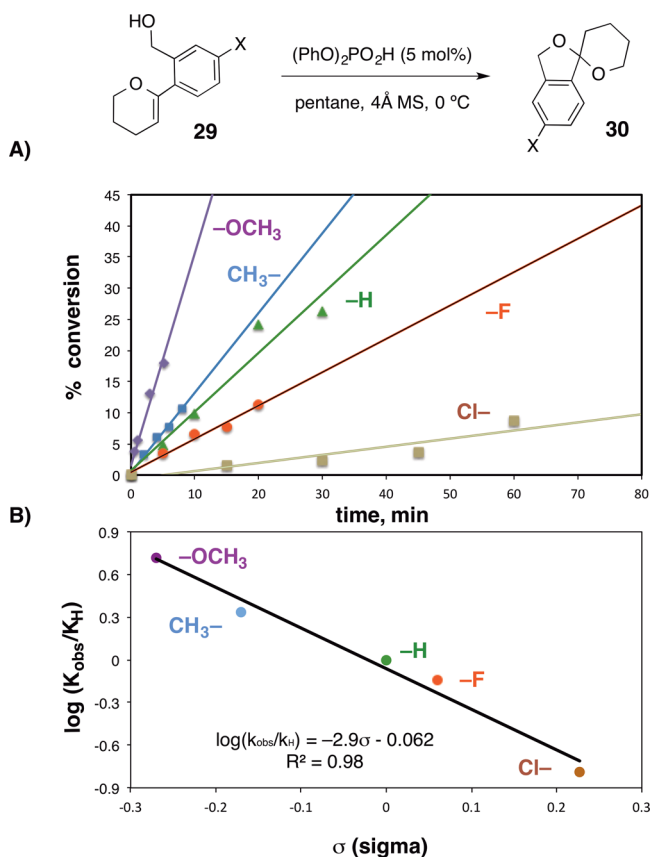


Figure 2. Hammett analysis of (PhO)₂PO₂H-catalyzed spiroketalization of **29**. (A) Rates of conversion of **29** with (PhO)₂PO₂H (5 mol %) as the catalyst in pentane at 0 °C. (B) Hammett plot exhibiting a linear correlation for the electronically varied substrates **29** ($\rho = -2.9$).

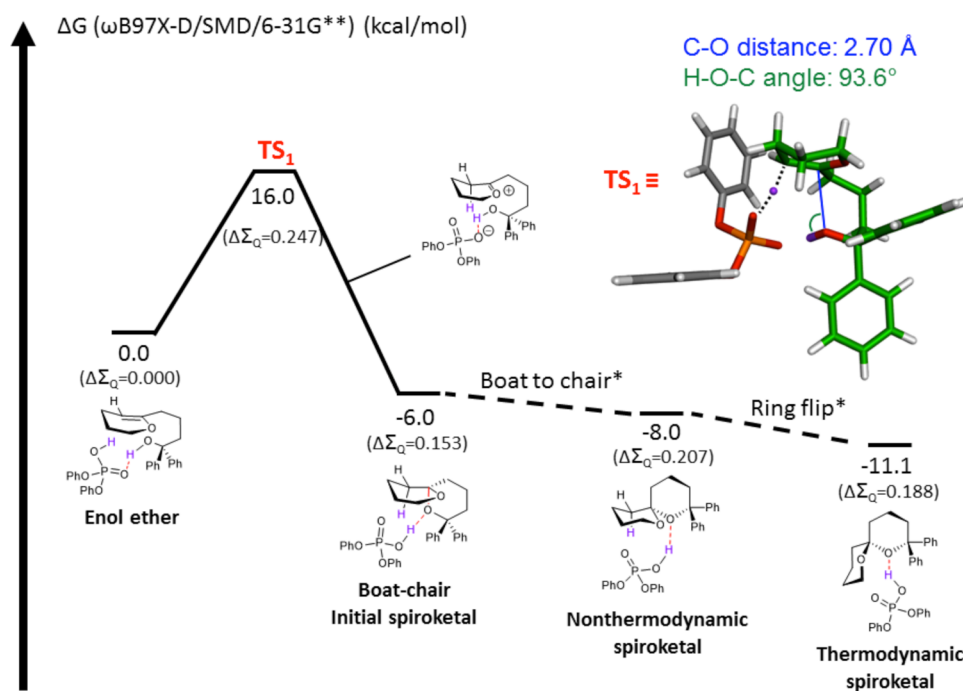


Figure 3. Concerted asynchronous mechanism for the ring closure of the 6,6-spiroketalization model system. The values in parentheses correspond to the differences in the sum of the Mulliken charges on the enol ether oxygen and electrophilic carbon with respect to the starting complex. Barriers indicated by * were not calculated.

through a chiral phosphate acetal intermediate.^{13d} In the piperidine formation mechanism and the present spiroketalization, GSM is especially useful in locating challenging asynchronous and concerted transformations because of its flexible treatment of the reaction pathway tangent vector (for details, see the [Supporting Information](#)). Prior to the use of GSM to locate reaction pathways, a preliminary study of the diphenyl hydrogen phosphate-catalyzed spiroketalization of a simplified enol ether leading to 1,7-dioxaspiro[5.5]undecane was performed using the Zimmerman group's combinatorial reaction discovery procedure.^{23b,e} The results suggested that the concerted pathway could compete with the phosphate-mediated and S_N1 -like mechanisms.

Following these preliminary results, more rigorous studies were performed that involved an initial extensive exploration of possible orientations of the catalyst–product complex for three different systems: the diphenyl phosphoric acid **26**-catalyzed 6,6-spiroketalization, the **26**-catalyzed 6,5-spiroketalization, and the chiral CPA **7a**-catalyzed 6,6-spiroketalization. Reaction path exploration and exact transition state searches were performed using GSM for each of the three types of mechanisms shown in [Scheme 3](#). The resultant intermediates and transition states were corrected for thermodynamics and solvent effects (pentane). Reported energies are solvent-phase free energies with thermodynamic corrections at 298 K (diphenyl hydrogen phosphate catalyst system) and 238 K (**7a** catalyst system) obtained at the ω B97X-D/SMD/6-31G** level.

To discriminate between the three mechanisms shown in [Scheme 3](#), the transformation leading to a 6,6-spiroketal (substrate **6a**) was investigated first using a model diphenyl hydrogen phosphate catalyst. While this initial study did not use a chiral catalyst, the lowest-barrier pathway unveiled by these simulations was further examined with the full catalyst (vide infra). Before examining the phosphate-mediated and oxocarbenium pathways, 12 concerted pathways leading to thermody-

amic and nonthermodynamic spiroketals were investigated. The most favored pathway produces a nonthermodynamic spiroketal (only one anomeric effect present) that can readily convert to the more stable thermodynamic spiroketal, as shown in [Figure 3](#). The reaction pathway is concerted and asynchronous: from the substrate alcohol to phosphate H-bonded complex, an initial protonation of the enol ether occurs at the transition state (TS_1). Additionally, the transition state shows a chairlike geometry involving the alcohol oxygen and the electrophilic carbon with a C–O distance of 2.70 Å. After the transition state, synchronous deprotonation and cyclization occur. The initial spiroketal is formed in a chair-boat conformation, which can readily rearrange to a more stable nonthermodynamic chair–chair conformation and ultimately, by a ring flip, to the most thermodynamically stable spiroketal. The Mulliken charges on the enol ether oxygen and electrophilic carbon (provided in [Figure 3](#)) show a significant buildup of positive charge at TS_1 ($\Delta\Sigma_Q = 0.247$) that is slightly smaller than the sum of charges of a bare oxocarbenium ion solvated in *n*-pentane ($\Delta\Sigma_Q = 0.271$; see the [Supporting Information](#)). The activation barrier for this transformation was 16.0 kcal/mol above the catalyst–substrate complex, which is fully consistent with a mechanism operative at or below room temperature. It should be noted that the dual function of the phosphoric acid as both a Brønsted acid and a Lewis base is efficiently exploited in this mechanism, as is evident in the rate-determining TS shown in [Figure 3](#). Although the product initially formed is predicted to be the nonthermodynamic spiroketal, this is only relevant in conformationally locked systems such as the glucal derivatives shown in [Scheme 2](#), since otherwise the thermodynamic spiroketal is readily accessed by a ring flip.

The anomeric phosphate-mediated pathway was also examined using the diphenyl catalyst model system, and different orientations of the catalyst were explored for this

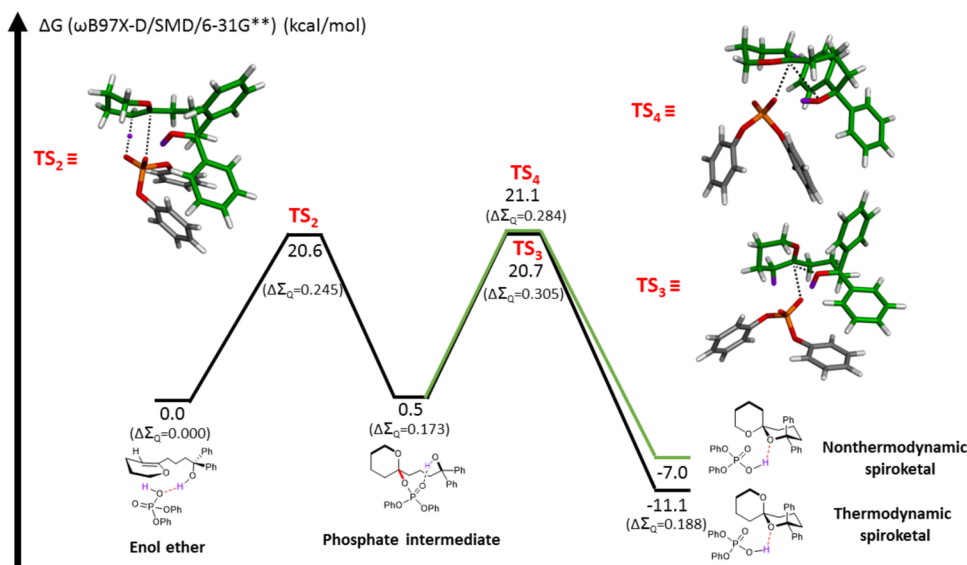


Figure 4. Anomeric phosphate mechanism for the 6,6-spiroketalization model system. The energies of important stationary points are shown in kcal/mol. The values in parentheses correspond to the differences in the sum of the Mulliken charges on the enol ether oxygen and electrophilic carbon with respect to the starting complex.

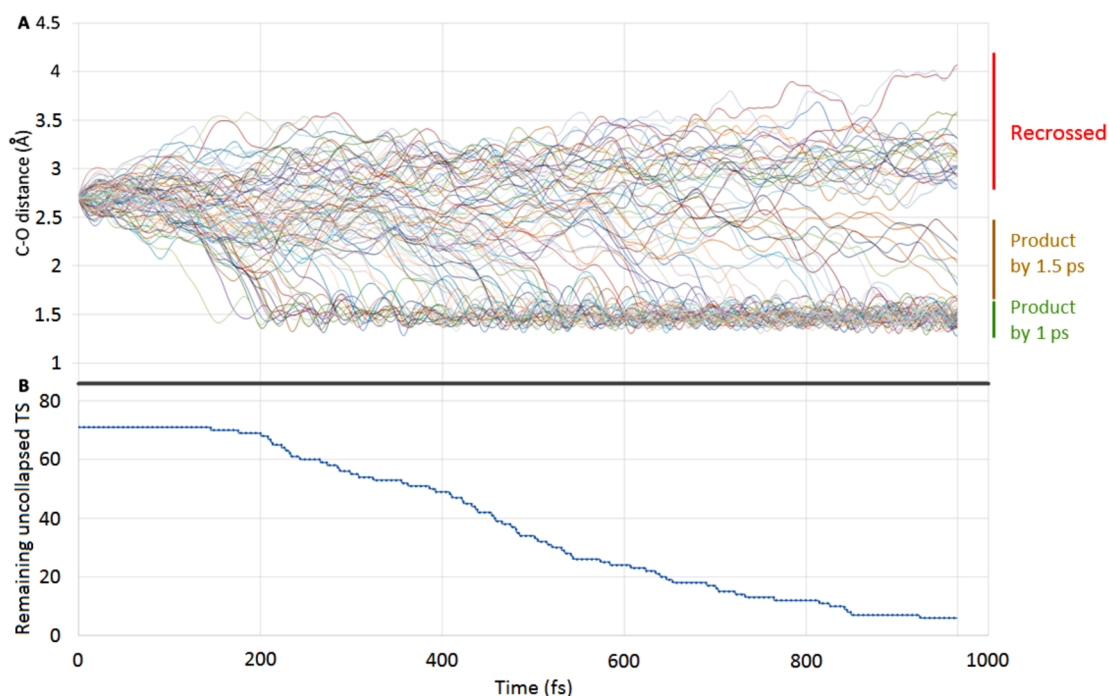


Figure 5. Results of the molecular dynamics calculations on the TS of the concerted pathway for the 6,6-spiroketalization of the model system. Each line represents one of the 100 independent runs. **A.** The new ring's C–O distance is plotted against time. **B.** The number of productive (71), but yet uncollapsed TSs is plotted against time.

mechanism. The attack of each phosphate oxygen was examined, and the lowest-energy pathway relevant to this mechanism is depicted in Figure 4. The initial orientation of the catalyst is similar to the concerted pathway described above, but the alcohol is not positioned in such a way that ring closure can readily occur. The formation of the anomeric phosphate intermediate instead proceeds through a concerted asynchronous mechanism. As initial protonation of the enol ether creates an ionic transition state and the alcohol moiety is further away from the electrophilic site, attack of the hydrogen-bonded oxygen of the phosphate can form an axial bond. The

formation of the phosphate intermediate has a barrier of 20.6 kcal/mol (TS_2), and its syn displacement by the nucleophilic alcohol to afford the spiroketal has a barrier of 20.7 kcal/mol (TS_3) (the anti phosphate displacement likely involves more than one phosphate and was not modeled). Once the phosphate intermediate is formed, there is not a large preference for the immediate formation of a thermodynamic as opposed to a nonthermodynamic spiroketal. In fact, although Figure 4 shows the sequence for the formation of the thermodynamic spiroketal, the phosphate could collapse to

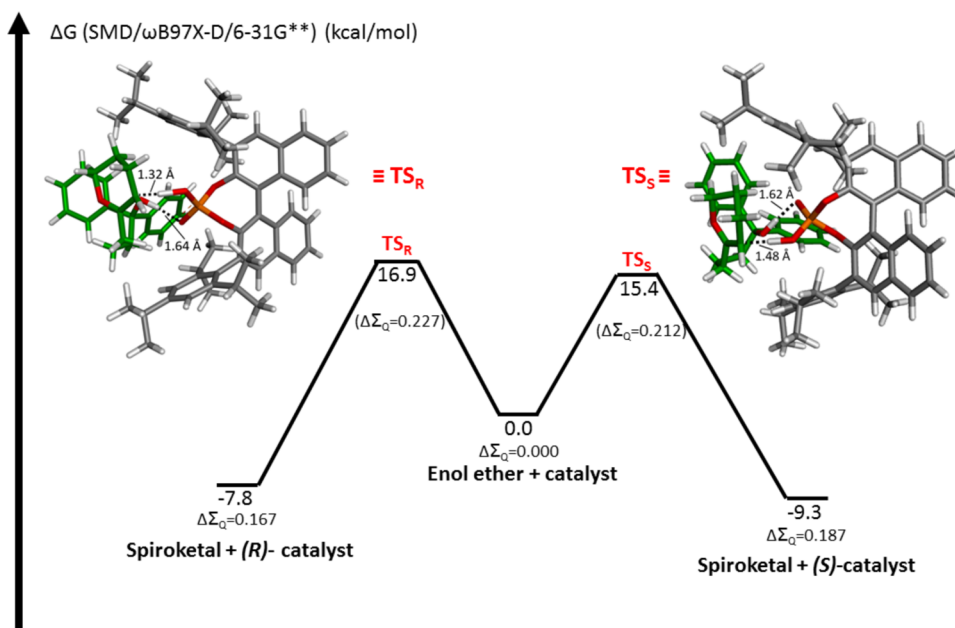


Figure 6. Comparison of the activation barriers for the (*R*)- and (*S*)-7a-catalyzed spiroketalizations. The insets depict the transition state structures. The values in parentheses correspond to the differences in the sum of the Mulliken charges on the enol ether oxygen and electrophilic carbon with respect to the starting complex.

form a nonthermodynamic spiroketal (TS_4) with a barrier of 21.1 kcal/mol.

The difference of 4.6 kcal/mol between the barriers for the concerted and anomeric phosphate mechanisms suggests that the phosphate mechanism is uncompetitive. To determine whether the concerted mechanism was also operative for five-membered-ring formation, reactions leading to a 6,5-spiroketal (**21c**) were examined. The relevant stationary points of the potential energy surface (PES) are shown in the [Supporting Information](#). Not surprisingly, the data show that the concerted mechanism ($E_a = 13.8$ kcal/mol) is favored over the anomeric phosphate path ($E_a = 22.9$ kcal/mol for spiroketal formation by syn displacement of the phosphate intermediate). The buildup of positive charge on the substrate and the asynchronicity of the changes in bonding are similar to those in the 6,6-spiroketalization. Finally, the KIE of 0.96 calculated for the concerted mechanism was in qualitative agreement with the experimentally measured value of 0.85.

The study of an oxocarbenium-mediated mechanism proved challenging because repeated efforts to optimize stationary points for oxocarbenium intermediates resulted in their collapse to the reactant or product structures. This observation, however, makes sense in light of the proposed concerted mechanism for spiroketalization, where the TS itself is ionic (oxocarbenium-like). Given that an unstable oxocarbenium-like structure is initially formed along the concerted path, we turned to molecular dynamics (MD) simulations to quantify the lifetime of this structure. If a stable oxocarbenium intermediate were possible, it would form after protonation of the substrate and could be identified by MD simulations following the protonation TS. Therefore, trajectories were sampled using quasiclassical initial velocities starting at the concerted TS structure to accurately mimic the experimental conditions (for details, see the [Supporting Information](#)). The plot of the C–O distance against time for the product's new C–O connection ([Figure 5A](#)) shows how most of the 100 MD runs proceed from the TS to the product. After removal of the trajectories

that recrossed to the reactant species, [Figure 5B](#) shows the progression of product-forming trajectories to the ring-closed structures. Of the 71 runs that resulted in product, an average time of 519 fs was required to form the spiroketal. No persistent oxocarbenium species were formed in any of the trajectories, including seven trajectories that needed to be run to 1.5 ps in order to complete product formation. This short time frame is consistent with the concerted asynchronous mechanism derived by GSM without a stable intermediate along the pathway. Additionally, the trajectories show that the alcohol deprotonation and ring closure occur synchronously, also in agreement with the reaction path from GSM. This occurs as a result of activation of the alcohol by the Lewis basic anionic oxygen of the catalyst, which quenches the buildup of positive charge on the alcohol oxygen by simultaneously deprotonating it while it forms the C–O bond.

Having established a concerted yet asynchronous mechanism for spiroketalization with the model diphenyl catalyst system, we next studied the reactions of substrate **6a** and chiral phosphoric acid **7a**. Specifically, formation of the (*R*)-spiroketal was modeled to determine the key interactions dictating the stereoselectivity of the reaction. Orientations of the catalyst analogous to those in the diphenyl phosphoric acid system were considered. To our delight, we found a 1.5 kcal/mol difference between the lowest computed activation barriers for the (*R*)-7a-catalyzed and (*S*)-7a-catalyzed concerted spirocyclizations, with the *S* catalyst chirality being favored (see [Figure 6](#)). Since the (*R*)-spiroketal was the designated simulation product, this result is in agreement with the chirality of the product formed in the experiment. Using a temperature of 238 K, we proceeded to calculate the expected enantiomeric excess, which is given by

$$ee = \frac{\exp\left(\frac{\Delta G^{TS}}{RT}\right) - 1}{\exp\left(\frac{\Delta G^{TS}}{RT}\right) + 1}$$

where ΔG^{TS} is the energy gap, R is the gas constant, and T is the absolute temperature. The computed enantiomeric excess is 92%, which exactly matches the experimental result.^{11b}

While this is a very promising result, it is only accurate because the intrinsic errors in quantum-chemical simulation have largely canceled one another out. However, this agreement has been seen in other applications of quantum-chemical methods to a number of stereoselective transformations.²⁴ The extensive study of the PES by careful sampling of the driving coordinates and the end points of the strings, which included five different approaches of the catalyst to produce either thermodynamic (two axial C–O bonds) or nonthermodynamic (two equatorial C–O bonds and both combinations of 1 axial and 1 equatorial C–O bond) spiroketals, as well as the fact that the comparison between the lowest-energy pathways for the two catalyst chiralities gives the proper selectivity, gives us confidence in our method and results.

A description of the predicted mechanism and its associated stereochemical model follows. In the first step of the predicted concerted asynchronous mechanism, the catalyst, irrespective of its chirality, is initially oriented in such a way that the phosphate oxygen can hydrogen-bond with the tertiary alcohol, while the Brønsted acidic hydrogen is aligned to add to the enol ether. As with the diphenyl catalyst model system, protonation of the enol ether occurs at the transition state for both catalyst chiralities. Also coherent with the diphenyl system, there is a considerable buildup of positive charge on the substrate at the TS compared with the enol ether–catalyst complex, in agreement with the experimental data on the mechanism (Hammett and secondary KIE experiments). For both catalyst chiralities, deprotonation of the nucleophilic oxygen and spirocyclization occur simultaneously following protonation, as observed for the diphenyl hydrogen phosphate model system. The cyclization occurs through a six-membered chair geometry to produce an initial boat-chair spiroketal that initially relaxes to a nonthermodynamic spiroketal and finally, by means of a ring flip, to the thermodynamic conformation. The relevant stationary points on the PES, disregarding the boat-chair spiroketal and the later isomerization to a thermodynamic product, are shown in Figure 6. While in this case the conformation of the immediately formed spiroketal is not vital (its equilibration to a more stable conformer is unimpeded), in conformationally locked structures it would be of importance. This mechanism shows how CPA catalysis can be used to form nonthermodynamic spiroketals with kinetic control. A major difference between the TS structures that explains the kinetic origin of the enantioselectivity is the interaction of the 2,4,6-triisopropylphenyl groups at the 3- and 3'-position of 7a with the phenyl rings of the tertiary alcohol of the substrate. Figure 7 shows the quadrant-based frontal perspective commonly used in stereochemical models involving CPAs and popularized by Himo²⁵ and Terada.²⁶ From this perspective, the diastereomeric relationship of the substrate–(*R*)-TRIP (TS_R) and substrate–(*S*)-TRIP (TS_S) spiroketalization TSs is made clear. At the TS, the substrate is arranged in such a way that protonation of the enol ether can take place, yet the positive charge being built in the electrophilic carbon is stabilized by its interaction with the alcohol oxygen. This is best achieved when the alcohol appendage adopts a chairlike geometry (Figure 7, top left diagram), in preparation for the asynchronous cyclization, and the phenyl rings are not located in the bulky quadrants near the catalytic site. To achieve this, the dihydropyran core is arranged in a different orientation for

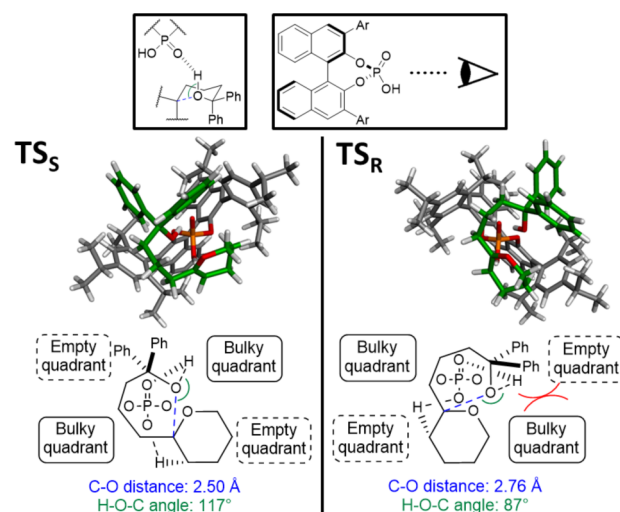


Figure 7. Comparison of concerted asynchronous mechanisms leading to the formation of an (*R*)-spiroketal involving (*S*)-7a (TS_S) and (*R*)-7a (TS_R).

TS_R and TS_S . The alcohol-containing side chain in TS_R adopts a less ideal chairlike geometry because of unfavorable steric interactions between the phenyl rings of the substrate and the ortho and para substituents on the aryl groups of the CPA. This is reflected by a longer distance between the nucleophilic oxygen and the electrophilic carbon (2.76 Å for TS_R vs 2.50 Å for TS_S) and a less directed angle for electronic interaction (87° H–O–C angle for TS_R vs 117° for TS_S). Figure 8 provides a

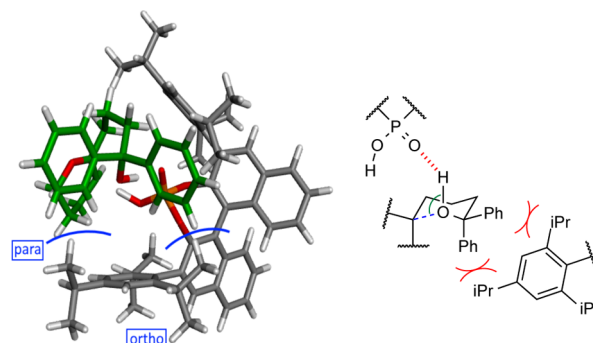


Figure 8. Key steric interactions at TS_R between the phenyl groups on the alcohol appendage of the enol ether and the ortho and para substituents of the aryl substituents of (*R*)-7a.

perspective focusing on these key steric interactions in TS_R . Substitution of the phenyl rings on the tertiary alcohol with more flexible benzyl groups would be expected to relieve the steric congestion at TS_R and result in a decreased ee, as observed experimentally.

CONCLUSION

This article describes the development of chiral phosphoric acid-catalyzed stereoselective spiroketalizations as well as mechanistic and computational studies of the mechanistic origins of catalysis. The commercially available TRIP catalysts were found to be effective promoters of the enantioselective formation of chiral spiroketals and diastereoselective formation of non-anomeric spiroketals. The reactions were found to proceed under kinetic control, where nonpolar solvents (i.e., pentane) and anhydrous conditions (4 Å MS as additives) were

found to be essential for attaining high levels of stereocontrol. The experimental studies were designed to differentiate between the S_N1 -like, S_N2 -like, and covalent phosphate intermediate-based mechanisms. The chiral phosphoric acid-catalyzed spiroketalization of deuterium-labeled cyclic enol ethers revealed a highly diastereoselective syn-selective protonation/nucleophile addition, thus ruling out long-lived oxocarbenium intermediates. At the same time, the intermolecular equivalent of these reactions (i.e., tetrahydropyranylation with D3-labeled dihydropyran) was found to proceed unselectively, presumably by a different (i.e., S_N1 -like) mechanism. Hammett analysis of the reaction kinetics revealed accumulation of positive charge in the transition state of the rate-limiting step ($\rho = -2.9$), and the KIE for the spiroketalization with D-labeled substrates was determined to be 0.85. The subsequent in-depth computational studies on the phosphoric acid-catalyzed spiroketalization mechanism suggested that a single-step asynchronous mechanism is responsible for the observed experimental data. This mechanism fully exploits the bifunctionality of the catalyst and is novel for this type of transformation.¹⁵ The anomeric phosphate pathway was shown to have higher energy barriers. Additionally, molecular dynamics simulations showed the average lifetime of oxocarbenium structures to be 519 ± 240 fs, which does not support the formation of a stable ionic intermediate. The stereoselectivity of the reaction was examined in a complete system, and the key interactions that favor the experimentally observed results were identified to be linked with the 3,3'-aryl substituents of the CPA and the substituents on the alcohol group of the substrate. This stereochemical model was highly consistent with the observed experimental results in terms of the selectivity and the level of enantiocontrol, and this will allow not only future catalyst design to overcome the procedure limitations and expand its scope, but also the analysis of related reactions, such as intermolecular chiral phosphoric acid-catalyzed formation of acetal/aminal/hemiaminal ethers from enol ethers. Finally, the applicability of the growing string method for the analysis of hydrogen-bond organocatalytic transformations involving large systems was demonstrated, as was its usefulness in the proposal of the underlying mechanism and in the explanation of the stereocontrol observed.

■ ASSOCIATED CONTENT

● Supporting Information

The Supporting Information is available free of charge on the ACS Publications website at DOI: 10.1021/jacs.5b12528.

Experimental procedures; detailed description of computational studies; ^1H , ^2H , and ^{13}C NMR spectra; and HPLC traces (PDF)

■ AUTHOR INFORMATION

Corresponding Authors

*nagorny@umich.edu

*paulzim@umich.edu

Notes

The authors declare no competing financial interest.

■ ACKNOWLEDGMENTS

We dedicate this paper to Prof. James D. White on the occasion of his 80th birthday. This work was supported by a National Science Foundation CAREER Award (CHE-1350060). P.N. is a Sloan Foundation and Amgen Young Investigator Fellow. We

thank Dr. Yong Guan for help with the synthesis of substrates 20 and 21 and David Braun for computational support.

■ REFERENCES

- (1) (a) Perron, F.; Albizzati, K. F. *Chem. Rev.* **1989**, *89*, 1617. (b) Mitsunishi, S.; Shima, H.; Kawamura, T.; Kikuchi, K.; Oikawa, M.; Ichihara, A.; Oikawa, H. *Bioorg. Med. Chem. Lett.* **1999**, *9*, 2007. (c) Uckun, F. M.; Mao, C.; Vassilev, A. O.; Huang, H.; Jan, S.-T. *Bioorg. Med. Chem. Lett.* **2000**, *10*, 541. (d) Huang, H.; Mao, C.; Jan, S.-T.; Uckun, F. M. *Tetrahedron Lett.* **2000**, *41*, 1699.
- (2) Booth, Y. K.; Kitching, W.; De Voss, J. J. *Nat. Prod. Rep.* **2009**, *26*, 490.
- (3) Dominguez, H. J.; Paz, B.; Daranas, A. H.; Norte, M.; Franco, J. M.; Fernandez, J. J. *Toxicol.* **2010**, *56*, 191.
- (4) Deslongchamps, P. *Stereoelectronic Effects in Organic Chemistry*; Pergamon Press: Oxford, U.K., 1983.
- (5) (a) Gallimore, A. R.; Stark, C. B. W.; Bhatt, A.; Harvey, B. M.; Demydchuk, Y.; Bolanos-Garcia, V.; Fowler, D. J.; Staunton, J.; Leadlay, P. F.; Spencer, J. B. *Chem. Biol.* **2006**, *13*, 453. (b) Takahashi, S.; Toyoda, A.; Sekiyama, Y.; Takagi, H.; Nogawa, T.; Uramoto, M.; Suzuki, R.; Koshino, H.; Kumano, T.; Panthee, S.; Dairi, T.; Ishikawa, J.; Ikeda, H.; Sakaki, Y.; Osada, H. *Nat. Chem. Biol.* **2011**, *7*, 461.
- (6) (a) Boivin, T. L. B. *Tetrahedron* **1987**, *43*, 3309. (b) Mead, K. T.; Brewer, B. N. *Curr. Org. Chem.* **2003**, *7*, 227. (c) Raju, B. R.; Saikia, A. K. *Molecules* **2008**, *13*, 1942. (d) Sperry, J.; Liu, Y.-C.; Brimble, M. A. *Org. Biomol. Chem.* **2010**, *8*, 29. (e) Cala, L.; Fananas, F. J.; Rodriguez, F. *Org. Biomol. Chem.* **2014**, *12*, 5324.
- (7) (a) Aho, J. E.; Pihko, P. M.; Rissa, T. K. *Chem. Rev.* **2005**, *105*, 4406. (b) Favre, S.; Vogel, P.; Gerber-Lemaire, S. *Molecules* **2008**, *13*, 2570. (c) Sous, M. E.; Ganame, D.; Zanatta, S.; Rizzacasa, M. A. *ARKIVOC* **2006**, 2006 (vii), 105.
- (8) For an overview of transition-metal-catalyzed formation of spiroketals, see: (a) Palmes, J. A.; Aponick, A. *Synthesis* **2012**, *44*, 3699.
- (9) For representative approaches to kinetic spiroketals, see: (a) Pihko, P. M.; Aho, J. E. *Org. Lett.* **2004**, *6* (21), 3849. (b) Takaoka, L. R.; Buckmelter, A. J.; LaCruz, T. E.; Rychnovsky, S. D. *J. Am. Chem. Soc.* **2005**, *127*, 528. (c) LaCruz, T. E.; Rychnovsky, S. D. *Org. Lett.* **2005**, *7* (9), 1873. (d) Potuzak, J. S.; Moilanen, S. B.; Tan, D. S. *J. Am. Chem. Soc.* **2005**, *127*, 13796. (e) Moilanen, S. B.; Potuzak, J. S.; Tan, D. S. *J. Am. Chem. Soc.* **2006**, *128*, 1792. (f) Vellucci, D.; Rychnovsky, S. D. *Org. Lett.* **2007**, *9* (4), 711. (g) Castagnolo, D.; Breuer, I.; Pihko, P. M. *J. Org. Chem.* **2007**, *72* (26), 10081. (h) Liu, G.; Wurst, J. M.; Tan, D. S. *Org. Lett.* **2009**, *11* (16), 3670. (i) Sharma, I.; Wurst, J. M.; Tan, D. S. *Org. Lett.* **2014**, *16*, 2474.
- (10) For representative auxiliary-based approaches to chiral spiroketals, see: (a) Iwata, C.; Hattori, K.; Uchida, S.; Imanishi, T. *Tetrahedron Lett.* **1984**, *25* (28), 2995. (b) Iwata, C.; Fujita, M.; Hattori, K.; Uchida, S.; Imanishi, T. *Tetrahedron Lett.* **1985**, *26* (18), 2221. (c) Uchiyama, M.; Oka, M.; Harai, S.; Ohta, A. *Tetrahedron Lett.* **2001**, *42* (10), 1931. (d) Wu, K.-L.; Wilkinson, S.; Reich, N. O.; Pettus, T. R. R. *Org. Lett.* **2007**, *9* (26), 5537. Aitken, H. R. M.; Furekert, D. R.; Hubert, J. G.; Wood, J. M.; Brimble, M. A. *Org. Biomol. Chem.* **2013**, *11*, 5147.
- (11) For catalyst-controlled asymmetric spiroketalization reactions, see: (a) Coric, I.; List, B. *Nature* **2012**, *483*, 315. (b) Sun, Z.; Winschel, G. A.; Borovika; Nagorny, P. A. *J. Am. Chem. Soc.* **2012**, *134*, 8074. (c) Nagorny, P.; Sun, Z.; Winschel, G. A. *Synlett* **2013**, *24*, 661. (d) Quach, R.; Furekert, D. P.; Brimble, M. A. *Tetrahedron Lett.* **2013**, *54*, 5865. Wu, H.; He, Y.-P.; Gong, L.-Z. *Org. Lett.* **2013**, *15*, 460. (e) Wang, X.; Guo, P.; Wang, X.; Wang, Z.; Ding, K. L. *Adv. Synth. Catal.* **2013**, *355*, 2900. (f) Cala, L.; Mendoza, A.; Fananas, F. J.; Rodriguez, F. *Chem. Commun.* **2013**, *49*, 2715. (g) Wang, F.; Chen, F.; Qu, M.; Li, T.; Liu, Y.; Shi, M. *Chem. Commun.* **2013**, *49*, 3360. (h) Rexit, A. A.; Mailikezati, M. *Tetrahedron Lett.* **2015**, *56*, 2651.
- (12) For catalyst-controlled acetalization reactions, see: (a) Nagano, H.; Katsuki, T. *Chem. Lett.* **2002**, *8*, 782–783. (b) Coric, I.; Vellalath, S.; List, B. *J. Am. Chem. Soc.* **2010**, *132*, 8536–8537. (c) Coric, I.; Muller, S.; List, B. *J. Am. Chem. Soc.* **2010**, *132*, 17370–17373. (d) Cox, D. J.; Smith, M. D.; Fairbanks, A. J. *Org. Lett.* **2010**, *12*, 1452.

- (e) Rubush, D. M.; Morges, M. A.; Rose, B. J.; Thamm, D. H.; Rovis, T. *J. Am. Chem. Soc.* **2012**, *134*, 13554. (f) Kim, J. H.; Coric, I.; Vellalath, S.; List, B. *Angew. Chem., Int. Ed.* **2013**, *52*, 4474. (g) Mensah, E.; Camasso, N.; Kaplan, W.; Nagorny, P. *Angew. Chem., Int. Ed.* **2013**, *52*, 12932. (h) Chen, Z.; Sun, J. *Angew. Chem., Int. Ed.* **2013**, *52*, 13593. (i) Kimura, T.; Sekine, M.; Takahashi, D.; Toshima, K. *Angew. Chem., Int. Ed.* **2013**, *52*, 12131. (j) Rubush, D. M.; Rovis, T. *Synlett* **2014**, 25, 713. (k) Yamanaka, T.; Kondoh, Z.; Terada, M. *J. Am. Chem. Soc.* **2015**, *137*, 1048. (l) Kim, J. H.; Coric, I.; Palumbo, C.; List, B. *J. Am. Chem. Soc.* **2015**, *137*, 1778. (m) Matsumoto, A.; Asano, K.; Matsubara, S. *Chem. Commun.* **2015**, *51*, 11693. (n) Jiang, L.; Jia, T.; Wang, M.; Liao, J.; Cao, P. *Org. Lett.* **2015**, *17*, 1070. (o) Qian, H.; Zhao, W.; Wang, Z.; Sun, J. *J. Am. Chem. Soc.* **2015**, *137*, 560.
- (13) (a) Borovika, A.; Nagorny, P. *Tetrahedron* **2013**, *69*, 5719. (b) Borovika, A.; Tang, P.-I.; Klapman, S.; Nagorny, P. *Angew. Chem., Int. Ed.* **2013**, *52*, 13424. (c) Bhattarai, B.; Tay, J.-H.; Nagorny, P. *Chem. Commun.* **2015**, *51*, 5398. (d) Sun, Z.; Winschel, G. A.; Zimmerman, P.; Nagorny, P. *Angew. Chem., Int. Ed.* **2014**, *53*, 11194. (e) Tay, J. H.; Arguelles, A. J.; Nagorny, P. *Org. Lett.* **2015**, *17*, 3774.
- (14) (a) Rowland, G. B.; Zhang, H.; Rowland, E. B.; Chennamadhavuni, S.; Wang, Y.; Antilla, J. C. *J. Am. Chem. Soc.* **2005**, *127*, 15696–15697. (b) Liang, Y.; Rowland, E. B.; Rowland, G. B.; Perman, J. A.; Antilla, J. C. *Chem. Commun.* **2007**, 4477–4479. (c) Cheng, X.; Vellalath, S.; Goddard, R.; List, B. *J. Am. Chem. Soc.* **2008**, *130*, 15786–15787. (d) Li, G.; Fronczek, F. R.; Antilla, J. C. *J. Am. Chem. Soc.* **2008**, *130*, 12216–12217. (e) Rueping, M.; Antonchick, A. P.; Sugiono, E.; Grenader, K. *Angew. Chem., Int. Ed.* **2009**, *48*, 908–910. (f) Ingle, G. K.; Mormino, M. G.; Wojtas, L.; Antilla, J. C. *Org. Lett.* **2011**, *13* (18), 4822–4825.
- (15) (a) Pothier, N.; Goldstein, S.; Deslongchamps, P. *Helv. Chim. Acta* **1992**, *75*, 604. (b) Castagnolo, D.; Breuer, I.; Pihko, P. M. *J. Org. Chem.* **2007**, *72*, 10081.
- (16) (a) Lu, C.; Su, X.; Floreancig, P. E. *J. Org. Chem.* **2013**, *78*, 9366. (b) Kanomata, K.; Toda, Y.; Shibata, Y.; Yamanaka, M.; Tsuzuki, S.; Gridnev, I. D.; Terada, M. *Chem. Sci.* **2014**, *5*, 3515.
- (17) Shapiro, N. D.; Rauniyar, V.; Hamilton, G. L.; Wu, J.; Toste, D. F. *Nature* **2011**, *470*, 245.
- (18) Wurst, J. M.; Liu, G.; Tan, D. S. *J. Am. Chem. Soc.* **2011**, *133*, 7916.
- (19) Kotke, M.; Schreiner, P. R. *Synthesis* **2007**, 779.
- (20) (a) Bohe, L.; Crich, D. *Carbohydr. Res.* **2015**, *403*, 48. (b) Crich, D. *Acc. Chem. Res.* **2010**, *43*, 1144. (c) Bohe, L.; Crich, D. *C. R. Chim.* **2011**, *14*, 3. (d) Beaver, M. G.; Billings, S. B.; Woerpel, K. A. *Eur. J. Org. Chem.* **2008**, 2008, 771. (e) Smith, D. M.; Woerpel, K. A. *Org. Biomol. Chem.* **2006**, *4*, 1195. (f) Whitfield, D. M. *Adv. Carbohydr. Chem. Biochem.* **2009**, *62*, 83.
- (21) (a) Huang, M.; Garrett, G. E.; Birlirakis, N.; Bohe, L.; Pratt, D. A.; Crich, D. *Nat. Chem.* **2012**, *4*, 663. (b) Huang, M.; Retailleau, P.; Bohe, L.; Crich, D. *J. Am. Chem. Soc.* **2012**, *134*, 14746. (c) Crich, D.; Sharma, I. *J. Org. Chem.* **2010**, *75*, 8383. (d) Crich, D.; Vinogradova, O. *J. Org. Chem.* **2006**, *71*, 8473. (e) Crich, D.; Sun, S. *J. Am. Chem. Soc.* **1997**, *119*, 11217. (f) Crich, D.; Sun, S. *J. Org. Chem.* **1997**, *62*, 1198. (g) Crich, D.; Sun, S. *J. Org. Chem.* **1996**, *61*, 4506.
- (22) Butts, P. C.; Heise, B.; Tatolo, G. *Org. Lett.* **2012**, *14*, 3256.
- (23) (a) Zimmerman, P. M. *J. Comput. Chem.* **2013**, *34* (16), 1385–1392. (b) Zimmerman, P. M. *J. Chem. Phys.* **2013**, *138*, 184102. (c) Zimmerman, P. M. *J. Chem. Theory Comput.* **2013**, *9* (7), 3043–3050. (d) Zimmerman, P. M. *J. Comput. Chem.* **2015**, *36*, 601–611. (e) Zimmerman, P. M. *Mol. Simul.* **2015**, *41* (1–3), 43–54.
- (24) For selected applications of quantum-chemical methods in the study of stereoselective organocatalytic reactions, see: (a) Allemann, C.; Gordillo, R.; Clemente, F. R.; Cheong, P. H. Y.; Houk, K. N. *Acc. Chem. Res.* **2004**, *37*, 558–569. (b) Markad, S. D.; Xia, S.; Snyder, N. L.; Surana, B.; Morton, M. D.; Hadad, C. M.; Peczu, M. W. *J. Org. Chem.* **2008**, *73*, 6341–6354. (c) Schneebeli, S. T.; Hall, M. L.; Breslow, R.; Friesner, R. *J. Am. Chem. Soc.* **2009**, *131*, 3965–3973. (d) Krenske, E. H.; Houk, K. N. *Acc. Chem. Res.* **2013**, *46* (4), 979–989.